SECURITY INFORMATION

CONFIDENTIAL

Copy 6
RM E53F18

NACA RM E53F18

SEP 16 1953

NACA

RESEARCH MEMORANDUM

UTILIZATION OF EXTERNAL-COMPRESSION DIFFUSION PRINCIPLE IN DESIGN OF SHOCK-IN-ROTOR SUPERSONIC COMPRESSOR BLADING

By John W. R. Creagh and John F. Klapproth

Lewis Flight Propulsion Laboratory
Cleveland, Ohio

CLASSIFICATION CHANGED
UNCLASSIFIED
To _____

NACA Res abs
By authority of TRN-128 Date June 24, 1958
AMT 8-12-58

CLASSIFIED DOCUMENT

This material contains information affecting the National Defense of the United States within the meaning of the espionage laws, Title 18, U.S.C., Secs. 793 and 794, the transmission or revelation of which in any manner to an unauthorized person is prohibited by law.

NATIONAL ADVISORY COMMITTEE
FOR AERONAUTICS

WASHINGTON
September 11, 1953

NACA LIBRARY
LANGLEY AERONAUTICAL LABORATORY
Langley Field, Va.

CONFIDENTIAL

1P

NACA RM E53F18

NASA Technical Library
3 1176 01435 2612

2897

T-MC

NATIONAL ADVISORY COMMITTEE FOR AERONAUTICS

RESEARCH MEMORANDUM

UTILIZATION OF EXTERNAL-COMPRESSION DIFFUSION PRINCIPLE IN DESIGN OF SHOCK-IN-ROTOR SUPERSONIC COMPRESSOR BLADING

By John W. R. Creagh and John F. Klapproth

SUMMARY

The application of the external-compression principle to a cascade of blades in an attempt to achieve a closer approach to isentropic contraction ratios in supersonic compressor blading is presented. Limitations arising from the application to a cascade of blades are considered, and the limiting contraction ratio is shown to depend upon the inlet Mach number and the blade leading-edge wedge angle.

Tests of a rotor designed to incorporate the external-compression principle are presented. No improvement in performance was observed over previous shock-in-rotor compressors. The design inlet conditions for the rotor were not obtained because of an inadequate allowance for the blade leading-edge thickness. The observed contraction ratios were generally equal to or less than those observed in previous shock-in-rotor designs. No conclusions could be drawn regarding the use of the spike-diffuser principle to approach isentropic contraction ratios.

General considerations of shock-in-rotor compressor designs indicate that a more satisfactory design would distribute the static-pressure rise between a rotor and a stator. In addition, the design limitations such as observed with subsonic and transonic compressors as well as observed limitations on static-pressure rise through shocks before separation should also be considered in the design of supersonic compressors.

INTRODUCTION

The possibility of obtaining high-stage pressure ratios by using high wheel speeds and supersonic relative velocities in compressor blade rows has been recognized for a number of years (refs. 1 to 3). Several possible arrangements with supersonic velocities in the blade rows and with the shock positions in various locations have been considered (refs. 2, 4, and 5). The first arrangement receiving serious attention utilized supersonic relative inlet velocity and a normal shock in the rotor blade row with subsonic velocities in the subsequent stator (refs. 6 to 8).

In the initial design procedures for shock-in-rotor supersonic compressors, each passage was considered as an internal-compression-type supersonic diffuser; hence the design procedures were limited to the maximum recovery and contraction ratio (inlet area/throat area) associated with this diffuser type (ref. 9). Tests of rotors with the internal-compression diffuser principle yielded generally lower pressure ratios than predicted (refs. 6 and 10). The lower pressure ratios were attributed principally to a lack of subsonic diffusion in the rotor.

Attainment of design values of diffusion will require an improvement in the boundary-layer conditions at the start of the subsonic diffusion, that is, at the minimum section. A possible method of obtaining improvement is to reduce the Mach number at which the normal shock occurs by use of contraction ratios more nearly equal to the isentropic. A reduction in the minimum-section Mach number will not only reduce the free-stream total-pressure loss but can appreciably reduce the discontinuous static-pressure rise, which is generally responsible for flow separation.

2897

This report proposes the use of the spike- or Oswatitsch (ref. 11) diffuser principle for the design of supersonic compressor blading in order to more nearly approach the isentropic contraction ratio. A spike diffuser was designed to produce weak oblique compression waves ahead of the passage entrance; this principle was extended to compressor blading by properly contouring the trailing face of the blade to produce weak compression waves ahead of the blade-passage entrance. The starting requirements for a cascade of supersonic blading incorporating the spike-diffuser principle are considered and restrictions on the limiting contraction ratio are determined as a function of the blade leading-edge wedge angle and the relative entrance Mach number. Application of this principle to the design of a rotor blade is made and tests of the rotor in Freon-12 (dichlorodifluoromethane), a commercial refrigerant, are included.

The investigation was conducted at the NACA Lewis laboratory.

DESIGN CONSIDERATIONS

Application of External-Compression Principle to Cascades

For two-dimensional flow in a cascade with design operation and no standing bow-wave system (fig. 1), the incoming-flow direction will be parallel to AB on the trailing face of each blade (ref. 2). The trailing face is contoured from B to D so that compression waves arising from it intersect the leading edge of the following blade. This external-compression ramp is similar in purpose to the spike of a spike diffuser.

For spike diffusers, the Mach number is generally reduced as much as possible by means of the compression ramp. The principal restriction on the amount of diffusion arises from the condition that a standing bow wave on the outer shell or lip of the diffuser be avoided.

The standing bow-wave pattern may be avoided for the cascade of blades if the Mach number along AC on the driving face is very nearly 1.0 or above. The total effect of the changes in flow direction from upstream of the rotor to the minimum section should then be adjusted to give very nearly sonic velocities in the minimum section. Thus, if

ν Prandtl-Meyer angle

ϵ blade leading-edge wedge angle

φ change in blade angle from B to D

then

$$\nu_c = \nu_b - (\varphi + \epsilon) = \nu_a - (2\varphi + \epsilon) \approx 0$$

where the subscript a refers to the upstream condition, b refers to the condition on the compression ramp DF, and c refers to the condition at the minimum section.

The maximum change in angle on the compression ramp for a cascade of blades is then

$$\varphi \approx \frac{1}{2}(\nu_a - \epsilon)$$

so that, for any given inlet Mach number and leading-edge wedge angle, the change in angle of the compression ramp is fixed within close limits. The design wave configuration will then consist of a series of oblique compression waves from the compression ramp reflecting as an oblique shock from the driving face and reducing the Mach number to nearly 1.0. For Mach numbers on the compression ramp of 1.4 or below, the approximate signs can be replaced by an equality. However, for Mach numbers on the ramp above 1.4, the losses through the oblique shock reduce the change in angle $(\varphi + \epsilon)$ required to produce a Mach number of 1.0 behind the shock and must be accounted for in the design.

In order to obtain the design oblique shock AF (fig. 1), supersonic flow into the passage must be established. This requires that the minimum section be sufficiently large to pass the entire mass flow after suffering normal shock losses at the Mach number M_b. From the continuity equation in the form $PA\frac{A_{cr}}{A} = \text{constant}$ at any station, the

[redacted]

limiting contraction ratio for a Mach number of 1.0 at the minimum section is then (for definition of symbols see appendix A)

$$C = \frac{A}{A_{cr}}\bigg|_a \frac{P_c}{P_b} \tag{1}$$

where $\frac{A}{A_{cr}}\bigg|_a$ corresponds to M_a and P_c/P_b is the normal shock total-pressure recovery for M_b.

2897

Since the Mach number M_b is influenced by the leading-edge angle ϵ, the contraction ratio becomes a function of both entrance Mach number and ϵ. The theoretical limiting contraction ratio for several leading-edge wedge angles is shown for a range of Mach numbers in figure 2. In the calculation of the data for the curves shown, no allowance was made for boundary-layer effects. As shown in figure 2, closer approximation to isentropic contraction ratios may be obtained by using lower values of ϵ. It should be noted that the limitations of the contraction ratios of figure 2 will produce minimum-section areas larger than required for the design wave configuration. As a result, a slight reexpansion behind the oblique shock will occur, followed by a weak normal shock at the minimum section.

It is demonstrated in appendix B that, if the preceding method of determining contraction ratios is employed in the design of a cascade of blades, reduction in back pressure on the cascade is sufficient to permit starting from initial conditions with an extended wave system.

Application of External Compression to Rotor Design

The design of the supersonic portion of a rotor blade will require a matching of the flow conditions existing at successive radii. In order to avoid severe radial accelerations in the subsonic region, the pressure gradient at the minimum section should be close to that required for simple radial equilibrium

$$\frac{1}{\rho}\frac{dp}{dr} = \frac{V_\theta^2}{gr}$$

One method of obtaining a minimum-section Mach number of 1.0 and a balanced pressure gradient would be to use inlet guide vanes to establish the necessary relative inlet conditions. This method, however, results in a large gradient in inlet guide-vane turning angle, with a gradient appreciably greater than that required for a free vortex. A compressor designed with little or no guide-vane turning at the tip required such large guide-vane turning angles below root-tip radius ratios of about 0.75 that the axial Mach number and weight flow were seriously restricted.

[redacted]

A second method of balancing the pressure gradients at the minimum section would be to relieve the condition of a constant Mach number of 1.0 at this section. Minimum-section Mach numbers slightly below 1.0 may be obtained with a small amount of spillage, which will result in a slight increase in the shock losses at the region of spillage because of the extended wave pattern and a normal shock at the entrance instead of the more desirable strong oblique shock. For example, with an upstream inlet Mach number of 1.60 and a leading-edge wedge angle of 3°, a 1-percent spillage will reduce the relative total-pressure recovery from 0.980 for operation with a strong oblique shock (fig. 1) to 0.946 with a standing wave pattern and normal shock. The resultant minimum-section Mach number is reduced from 1.0 to 0.851 (see appendix B, fig. 17). A combination of guide-vane turning and spillage can obviously be used to establish radial equilibrium in order to avoid the use of excessive values of either.

2897

Rotor Design

The considerations of external compression were applied to the design of a supersonic compressor rotor with the following conditions specified:

Tip speed, ft/sec in air	1600
Inlet root-tip radius ratio	0.70
Absolute inlet Mach number at rotor tip	0.797

Inlet guide vanes were designed to produce turning which varied linearly from 3° at the tip to 20° at the hub, imparting a whirl component opposite to the direction of the rotor rotation. The resultant relative Mach number at the rotor inlet varied linearly from 1.548 at the root to 1.754 at the tip. Since the guide-vane turning at the hub was insufficient to establish simple radial equilibrium, a spillage of 1 percent at the hub was incorporated in the design.

The relative rotor-outlet conditions were selected to give a total-pressure ratio, with viscous losses neglected, of 2.70 with approximately equal work input along the radius. The relative outlet Mach number varie from 0.829 at the tip to 0.530 at the root. A blade trailing-edge and boundary-layer displacement thickness of 10 percent of the passage width was assumed at the blade outlet. The resultant relative discharge angle varied from 60.78° at the tip to 47.50° at the root. Turning in the rotor-blade passage varied from 2.20° at the tip to 12.75° at the root. In order to satisfy continuity, the root-tip radius ratio was increased from 0.70 at the inlet to 0.72 at the outlet.

The supersonic portion of the blade was designed as described for the cascade blade sections. An angle between the upstream flow direction

and the driving face of the blade ϵ averaging about 3.5° was used together with an assigned value of blade thickness near the leading edge of 0.040 to 0.046 inch for structural rigidity. The design inlet wave pattern for the pitch section is shown in figure 3. An arbitrary boundary-layer allowance of 0.015 inch per inch was made along the suction face of the blade.

The throat section was designed for a constant-flow area for a distance equal to one-half the passage width. The subsonic portion was designed to produce, along a streamline, a uniform increase in static-pressure rise corresponding to an equivalent 3.8° cone. The design vector diagrams in air for the tip, pitch, and root blade sections are shown in figure 4. Coordinates of the pitch section of the rotor blade are given in table I.

2897

APPARATUS AND INSTRUMENTATION

Compressor. - The compressor rotor used in this investigation is shown in figure 5. The rotor had 29 blades and a constant tip diameter from inlet to outlet of 16.0 inches. The axial depth of the rotor hub was 2.73 inches and the rotor-tip solidity was 2.33. The inlet guide-vane section contained 23 machined vanes constructed in accordance with the principles outlined in reference 12 and incorporated corrections for the secondary flows at the walls described in reference 13. The guide-vane solidity varied linearly from 1.68 at the root to 1.14 at the tip.

Variable-component test rig. - The experimental rotor of this investigation was installed in a variable-component test rig incorporating a closed gas-flow circuit for testing with Freon-12. The gas, after being compressed, passed consecutively through a pressure-reducing throttle and two sets of water-cooled heat exchangers and returned to a large tank (7.5 ft in diameter and 15 ft long) installed ahead of the compressor inlet. Automatic controls were provided to eliminate fluctuations in inlet temperature and pressure by regulating, respectively, the water flow to the heat exchangers and the rate of both pure Freon-12 addition to and test gas removal from the rig. The purity of the test gas was continuously recorded by use of a device similar to that described in reference 14 and adapted for use with Freon-12.

Power for driving the compressor was supplied by a 6000-horsepower variable-speed electric motor in conjunction with a speed increaser. The compressor test section of the rig is shown schematically in figure 6.

Instrumentation. - Standard instrumentation was installed in the large tank at the compressor inlet to measure pressures and temperatures according to the method described in reference 15. The compressor-outlet instrumentation at station 4 (fig. 6) used to obtain the over-all compressor performance consisted of two five-position shielded total-pressure

[redacted]

rakes and two five-position spike-type thermocouple rakes. The radial locations of the measuring stations on the rakes were such that values of the total pressure and the total temperature were obtained in the centers of five equal-annular areas. The rakes were set at an estimated mean value of flow angle and were insensitive to the variations in angle obtained in this investigation.

Radial surveys of angle of flow, total pressure, and static pressure were taken at stations 2 and 3 (fig. 6) by means of a cone-type probe. The static-pressure orifices on these probes were calibrated for the range of Mach numbers encountered. A more complete description of this type of probe is given in reference 16. Figure 7 shows a cone probe, a shielded total-pressure rake, and a spike-type thermocouple rake used in this investigation.

2897

Wall static pressures at stations 2, 3, and 4 were obtained by four equally spaced taps located on both the inner and outer walls. The static-pressure variation along the flow path through the rotor was measured by a series of wall taps located 0.1 inch apart on the outer casing and extending axially from a point corresponding to the axial location of the rotor-blade root at the inlet to the rotor-blade root at the outlet.

The weight flow of gas through the compressor was measured with an orifice installed in the piping downstream of the heat exchangers. Instrumentation at the orifice consisted of upstream and downstream wall-type static taps and an upstream temperature and total-pressure probe. In a preliminary investigation, the compressor test orifice was calibrated in air against a standard orifice, and the variation of the compressor-test-orifice flow coefficient with Reynolds number was established. During the subsequent compressor performance investigation, the Reynolds number at the orifice was calculated for each flow point. From the corresponding value of flow coefficient and with the use of the orifice instrumentation data in the standard orifice equation (ref. 17), the weight flow of test gas was obtained.

Total and static pressures in the compressor test rig were measured by a bank of mercury manometers. The pressure drop across the orifice was measured by a water manometer. Gas temperatures were determined by a potentiometer in conjunction with a precision galvanometer. The speed of the rotor was measured with an electric chronometric tachometer.

PROCEDURE

The over-all performance of the experimental rotor was obtained from tests in Freon-12. The design tip speed of 726 feet per second in Freon-12 was calculated by the method outlined in reference 16. Tests

were run at six rotational speeds from 50 to 100 percent of design equivalent tip speed in Freon-12 over a range of weight flows from open throttle to audible surge. During these tests the inlet-tank pressure was maintained constant at values between 29 and 32 inches of mercury absolute and the inlet-tank temperature was maintained constant at values between 75° and 100° F. Frequent checks were made to ensure the presence in the test rig of at least the minimum allowable test-gas purity of 97 percent Freon-12 by volume. Radial surveys were taken at stations 2 and 3 for the peak-efficiency flow point at design speed and at the maximum weight-flow point for all speeds. The total conditions in the entrance tank and at the compressor outlet (station 4) were used to determine the enthalpy rise for an isentropic process and for the actual process from the thermodynamic data for Freon-12 given in reference 18 (pp. 2577-2582). The adiabatic efficiency used in this investigation was equal to the ratio of the enthalpy increases for these two processes.

2897

RESULTS

Over-All Performance

The over-all performance of the compressor from open throttle to surge at six equivalent tip speeds from 50 to 100 percent of the design value is shown in figure 8. The maximum over-all total-pressure ratio of 2.24 occurred at design speed at a Freon-12 equivalent weight flow of 57.8 pounds per second and an adiabatic efficiency of 0.74. The maximum adiabatic efficiency of 0.755 was obtained at 90 percent of the design tip speed and at a weight flow of 52.8 pounds per second. The weight-flow range at tip speeds below 80 percent of the design speed was comparatively large but was sharply reduced at higher speeds until at design speed the variation in weight flow amounted to less than 1 percent of the maximum value. The peak total-pressure ratio obtained in this investigation was approximately 17 percent less than the design value of 2.70 and the weight flow at peak total-pressure ratio was approximately 3.3 percent below the design value of 59.8 pounds per second.

Performance at Design Speed and Peak Efficiency

Rotor-inlet surveys. - The results of the radial survey taken upstream of the rotor (station 2) are shown in figure 9 for peak efficiency at design equivalent speed. The experimental values of the inlet guide-vane turning angle are shown as a function of the radius together with the design values of the turning angle. It can be seen that the design values of turning were not achieved over most of the passage. At the root, the turning exceeded the design values by approximately 3°, but near the center of the passage and in the tip region the turning was closer to the design value. The difference between design and observed turning may be caused, in part, by the possible flow instabilities arising from the prescribed radial gradient in guide-vane turning.

The rotor-inlet conditions are shown in figure 10, where the relative inlet-flow angle, the axial inlet Mach number, and the relative inlet Mach number are plotted against the compressor radius. The corresponding design values of these parameters are also shown. The experimental values of the inlet-flow angle were greater than the design curve across the entire annulus, indicating that the gas entered the rotor at a positive angle of attack with a reduced axial velocity as shown by the Mach number curve. The variations from the design values of inlet guide-vane turning were not considered sufficient to account for the deficiency in the mass flow since the average values were near design. The relative inlet Mach numbers were lower than the design values, reflecting the effect of the low inlet axial velocities.

Rotor-outlet radial surveys. - The rotor-outlet-survey (station 3) data are shown in figure 11. The experimental and design values of the relative outlet-flow angle, the relative total-pressure recovery, and the relative outlet Mach number are plotted against the compressor radius. The relative outlet-flow angle was slightly less than design near the blade root, increased to values higher than design near mid-passage, and became so large near the tip that it exceeded the relative inlet-flow angle at this blade section. However, the observed energy input at the tip was large because of an appreciable reduction in the relative velocity.

The normal shock recoveries for the experimental values of the relative inlet Mach numbers are also shown in figure 11 together with the design and experimental relative total-pressure recovery. The design relative total-pressure recovery was obtained by considering only the losses through the design wave pattern and not viscous losses. The experimental and normal shock recoveries are approximately equal at the root and pitch sections of the blade passage, and both are lower than the design value. Near the tip region, however, the experimental curve fell below the normal shock curve and much lower than the design curve.

The experimental relative outlet Mach number in figure 11 was higher than the design value from the root to the midstream portion of the rotor-blade passage, indicating a lack of diffusion of the relative velocity in this area. Near the tip, the relative Mach number decreased to values lower than design. The low Mach number at the tip, however, was caused by the large losses in relative total pressure. The generally poor performance of the tip region indicated that either excessive losses occurred at the tip or that low-energy gas was centrifuged to the tip from the lower radii to cause the poor performance observed in the outer portion of the annulus. Similar conditions were observed in references 10 and 19.

2897

CW-2

Compressor weight-flow and static-pressure distribution. - The radial variations of weight flow at the inlet and outlet of the compressor are shown in figure 12. The nearly constant slope of the inlet curve indicated a generally uniform distribution of weight flow from root to tip and a nearly flat axial velocity profile across the flow passage. At the outlet, however, the gas flow shifted toward the root with the tip region carrying only a small portion of the total flow. This condition was also experienced in the investigation of the shock-in-rotor compressors of references 10 and 19.

The variation of the outer-wall static-pressure ratio along the flow path through the rotor is shown in figure 13. Because of the sweep of the rotor blades at the inlet and outlet of the compressor, the axial locations of the tip leading and trailing edges did not correspond to the leading and trailing edges at the blade root (fig. 5). As shown in figure 13, practically no static-pressure increase occurred at the outer wall until the gas entered the blade passage near the tip. Immediately thereafter, however, a rapid increase in static pressure was obtained, and the discharge static-pressure ratio ultimately attained a value of approximately 2.5.

2897

Off-Design Performance

Effect of compressor speed on relative inlet angle. - The variation of relative inlet-flow angle with relative inlet Mach number is shown in figure 14 for compressor operation at the maximum flow points for each of the several speeds at which radial surveys were taken. The experimental root-, pitch-, and tip-section performance are shown together with the values of blade stagger angles for these blade sections. The relative inlet-flow angles were reduced as the relative inlet Mach number increased above a value of approximately 1.2 with the pitch-section values of angle more nearly approaching the design values at design speed. The curves for all blade sections tended to flatten as design speed was approached, indicating that further increase in compressor speed could probably not be expected to produce any appreciable improvement in relative inlet angle characteristics.

DISCUSSION OF RESULTS

Inlet-flow conditions. - The operation of the rotor at design speed with an angle of attack did not permit the design wave pattern to be established. In order to determine the effect of the 0.040- to 0.046-inch blade thickness near the leading edge on the angle of attack, equation (B2) (appendix B) was solved by substituting the effective blade thickness in place of the spillage and by assuming an isentropic process. The resulting relative inlet-flow angles for design-speed operation were

62.75° at the root and 66.08° at the tip. Since these angles were close to the observed angles at the root and tip, the blade thickness near the leading edge is thought to be the principal reason for the experimental values of angle of attack. Further increases in speed over the design value should have little effect on the inlet-flow angle since, for an unchoked supersonic channel, the flow direction is fixed by the geometry of the blade leading-edge region ahead of the Mach line at the passage inlet (ref. 2).

2897

The effective contraction ratio for unit-passage height resulting from the observed inlet-flow angle

$$C = \frac{A_1}{A_{min}} = \frac{\frac{2\pi r}{n} \cos \beta_2'}{L}$$

is shown in figure 15 plotted against the relative inlet Mach number for the root, pitch, and tip radii for the maximum weight flow (i.e., no back pressure). The actual contraction ratio existing on the blade should be an average of the three conditions shown. The theoretical contraction ratio in Freon-12 for an external wave pattern with a 6° wedge angle (i.e., the average difference between the observed inlet-flow angle and the driving face) and the Kantrowitz contraction ratio are also shown. Near design speed, the observed ratios are below the Kantrowitz values. Because of the large blade stagger angles, small angles of attack produced relatively large changes in inlet-flow area and, hence, in the contraction ratio. Over the entire Mach number range of figure 15, the observed contraction ratios average slightly below the Kantrowitz values and no significant improvement in contraction ratio was observed over previous shock-in-rotor designs (refs. 6, 8, 10, and 19).

CW-2, back,

Rotor diffusion. - The relative outlet Mach numbers obtained with this rotor were about equal to those obtained with rotors designed for internal compression (refs. 10 and 19), which also exhibited poor subsonic diffusion. The shift in mass flow was also characteristic of the internal-compression rotors.

Improvement of the subsonic diffusion would require an improvement of flow conditions at the start of the subsonic diffusion (at the minimum section). Since the observed contraction ratios for this rotor are in general, equal to or less than those obtained in previous rotors, no conclusions can be drawn regarding possible improvement by exceeding the Kantrowitz limitations on the contraction ratio.

CONSIDERATIONS IN FUTURE DESIGNS

Permissible values of contraction ratio even with the external-compression principle do not allow the design of essentially shock-free flow, although appreciable improvement is theoretically obtainable over the internal-compression limitations. Recent observations (ref. 20) indicate that limits may exist on the maximum pressure rise that can be obtained through a shock without separation. This limitation may require minimum-section Mach numbers and oblique-shock strengths less than can be obtained by using the external-compression principle, particularly at the higher entrance Mach numbers.

2897

In addition to the limits on static-pressure rise through a shock, the over-all diffusion limitations observed on subsonic and transonic compressors (ref. 21) might also be expected to be significant for supersonic compressor designs. It is shown in reference 21 that for the tip section of conventional compressors, operation with values of a diffusion factor $D\left(D = 1 - \frac{V_3'}{V_2'} + \frac{\Delta V_\theta'}{2\sigma V_2'}\right.$ in the terminology of this report$\left.\right)$ above about 0.45 resulted in appreciable reduction in compressor efficiency. This limit is below the design value of 0.52 for the tip section of this rotor.

Consideration of the rotor as a component of a complete stage showed that a disproportionate unbalance would have existed between the static-pressure rise across the rotor and a stator blade row. The observed static-pressure ratio across the rotor (fig. 13) is greater than the observed total-pressure ratio. If stators were to be employed behind this rotor to return the flow to axial at the same absolute velocity as entered the rotor, no diffusion would be required across the stators.

On the basis of the above considerations, future shock-in-rotor designs should incorporate available information on static-pressure-rise limitations through shocks. In addition, the rotor design should be such that the over-all diffusion is within the limits of reference 21, at least until applicable limits are established for the supersonic region. An appreciable reduction in the required diffusion on the rotor will be obtained if the rotor is considered as a component of a complete stage and the static-pressure rise (expressed as D factor) is distributed over both rotor and stator.

Lewis Flight Propulsion Laboratory
National Advisory Committee for Aeronautics
Cleveland, Ohio, June 9, 1953

2897

APPENDIX A

SYMBOLS

The following symbols are used in this report:

A	area, sq ft
A/A_{cr}	ratio of flow area to critical area at any point
C	contraction ratio, $\frac{\text{inlet area}}{\text{throat area}}$
D	diffusion factor
g	acceleration due to gravity, 32.17 ft/sec^2
L	minimum distance between blades at throat section, ft
M	absolute Mach number, ratio of absolute gas velocity to local velocity of sound
M'	relative Mach number, ratio of gas velocity relative to rotor to local velocity of sound
n	number of rotor blades
P	total pressure of absolute gas flow, lb/sq ft
P'	total pressure of gas flow relative to rotor, lb/sq ft
p	static pressure, lb/sq ft
r	radius, ft
T	total temperature, $^{\circ}R$
U	rotor speed, ft/sec
V	absolute gas velocity, ft/sec
V'	gas velocity relative to rotor, ft/sec
W	weight flow, lb/sec
y	difference between maximum and actual stream tube height, ft (fig. 16)

[redacted]

β	angle between compressor axis and absolute gas-flow velocity, deg
β'	angle between compressor axis and gas-flow velocity relative to rotor, deg
δ	ratio of actual inlet total pressure to standard sea-level pressure, $P_1/2116$
ϵ	blade leading-edge wedge angle, deg
η	adiabatic efficiency
θ	ratio of actual inlet stagnation temperature to standard sea-level temperature, $T_1/518.4$
ν	Prandtl-Meyer angle, deg
ρ	density, lb/cu ft
σ	blade solidity
φ	change in blade angle at ramp section, deg

Subscripts:

a	upstream of rotor-blade ramp (fig. 1)
b	downstream of compression waves from blade ramp (fig. 1)
c	downstream of minimum section (fig. 1)
e	between bow wave and beginning of ramp section (fig. 16)
i	inlet to blade passage
min	throat section of blade passage (minimum section)
z	axial component
θ	tangential component
1	inlet tank
2	rotor inlet
3	rotor outlet
4	compressor-outlet rake station

2897

[redacted]

2897

APPENDIX B

ANALYSIS OF STARTING CHARACTERISTICS OF SUPERSONIC CASCADE WITH EXTERNAL COMPRESSION

In order to start a cascade of blades designed with the use of the contraction ratio given in equation (1), it must be shown that the extended wave pattern illustrated in figure 16 can be reduced and eliminated with only a change in back pressure. To eliminate this bow-wave system, the amount of spillage (or percentage of the maximum possible mass flow not entering the passage) from each blade passage must be reduced to zero. This can be accomplished with changes in back pressure only as long as the minimum-section Mach number remains less than 1.0. A sufficient condition then for starting the cascade is that the minimum-section Mach number should be less than 1.0 for all values of spillage.

The minimum-section Mach number resulting from a given amount of spillage can be obtained from the condition of continuity at the positions far upstream, at the passage entrance, and at the minimum section. Thus, from the use of the subscripts of figure 16 and with the boundary-layer effects neglected,

$$\rho_a V_a A_a = \rho_e V_e A_e = \rho_c V_c A_c \tag{B1}$$

where, for unit blade height,

$$A_a = \frac{2\pi r}{n} \cos \beta_a$$

$$A_c = \frac{2\pi r}{n} \frac{\cos \beta_e}{C}$$

$$A_e = \frac{2\pi r}{n} \cos \beta_e \left(1 - \frac{y}{\frac{2\pi r}{n} \cos \beta_e}\right)$$

The term $\left(1 - \frac{y}{\frac{2\pi r}{n} \cos \beta_e}\right)$ is the ratio of the actual flow area at the blade entrance to the maximum flow area (fig. 16), and C is the contraction ratio from region e to c for the design conditions (eq. (1))

Equation (B1) may be rewritten as

$$\left.\frac{A_{cr}}{A}\right|_a \frac{\cos \beta_a}{\cos \beta_e} = \left.\frac{A_{cr}}{A}\right|_e \left(1 - \frac{y}{\frac{2\pi r}{n} \cos \beta_e}\right) \frac{P_e}{P_a} \tag{B2}$$

and

$$\left.\frac{A_{cr}}{A}\right|_a \frac{\cos \beta_a}{\cos \beta_e} = \left.\frac{A_{cr}}{A}\right|_c \frac{P_c/P_a}{C} \tag{B3}$$

2897

Equation (B3) relates the minimum-section Mach number to the far upstream Mach number, the flow direction β_a, and the total-pressure recovery P_c/P_a through the extended wave system. For a given upstream Mach number, no convenient analytical relation could be found between β_a and P_c/P_a since the total-pressure recovery depends upon the amount of spillage $y/\frac{2\pi r}{n} \cos \beta_e$, the Mach number M_e, and the averaged total-pressure recovery through a branched-shock configuration at the passage entrance.

In order to investigate flow characteristics in the range of current rotor design values, numerical examples were selected by using for the design condition an axial inlet Mach number of 0.75, a leading-edge wedge angle of 3°, and inlet Mach numbers from 1.50 to 1.80. Solutions of equation (B3) were obtained for a range of far upstream flow angles β_a. The flow was first assumed to expand isentropically from β_a to the blade trailing-face angle β_e, and equation (B2) was solved to obtain an initial approximation to the required spillage. From this value of spillage and Mach number at region e, the losses through the extended wave pattern could be estimated from figure 4 of reference 22 and a corrected value of M_e obtained. The equation was then solved again to obtain a closer approximation to the required spillage. The process was repeated until the correct value of spillage was found which satisfied equation (B2). A very rapid convergence was obtained since, for the region of interest, the amount of spillage and consequently the total-pressure corrections were small.

The average total-pressure recovery from region e to region c (the minimum section) was obtained by a mass average of the recoveries through the shock system between these two stations. Part of the shock losses occurred at the reduced Mach number M_b behind the compression waves and part at the expanded Mach number M_e (fig. 16). A quantitative indication of the relative distribution of these two shock strengths

was obtained by the method of reference 23, in which it is shown that the location of the shock was a function principally of the Mach number and spillage. The total-pressure recovery from the far upstream region to the minimum section was then the product of the recoveries through the extended wave pattern and the recovery through the branched-shock system. Equation (B3) could then be solved and values of the minimum-section Mach number obtained.

The minimum-section Mach numbers obtained as outlined in the preceding discussion are plotted against percent spillage in figure 17. For the range of percent spillage shown, the data for all Mach numbers chosen fell within a narrow band. Figure 17 shows that for all values of percent spillage, the minimum-section Mach number was less than 1.0, thereby satisfying the previously discussed condition for starting the cascade with only changes in back pressure.

The ratio of the minimum-section static pressure to the upstream total pressure is also shown in figure 17. These curves reach a maximum when the losses through the wave system offset the static-pressure rise otherwise associated with the reduced minimum-section Mach number.

The effect of a boundary-layer displacement thickness at design operation would be to reduce the theoretical contraction ratio. If the displacement thickness increases as the shock is forced ahead of the passage (i.e., the spillage increased), the minimum-section Mach number will be raised over the ideal case shown in figure 17. If the increase became sufficiently large so as to raise the minimum-section Mach number to 1.0, further attempts to increase the spillage would lead to an impossible condition and the wave system must then break down.

REFERENCES

1. Weise, A. (G. J. Fabian, trans. and ed.): A Supersonic Axial Compressor. Pt. A., Vol. 9. Buships 338, Navy Dept., May 1946.

2. Kantrowitz, Arthur: The Supersonic Axial-Flow Compressor. NACA Rep. 974, 1950. (Supersedes NACA ACR L6D02.)

3. Wattendorf, Frank L.: High Speed Flow Through Cambered Rotating Grids. Jour. Aero. Sci., vol. 15, no. 4, Apr. 1948, pp. 243-247.

4. Wright, Linwood C., and Klapproth, John F.: Performance of Supersonic Axial-Flow Compressors Based on One-Dimensional Analysis. NACA RM E8L10, 1949.

2897 CW-3

[redacted]

5. Ferri, Antonio: Preliminary Analysis of Axial-Flow Compressors Having Supersonic Velocity at the Entrance of the Stator. NACA RM L9G06, 1949.

6. Erwin, John R., Wright, Linwood C., and Kantrowitz, Arthur: Investigation of an Experimental Supersonic Axial-Flow Compressor. NACA RM L6J01b, 1946.

7. Ritter, William K., and Johnsen, Irving A.: Performance of 24-Inch Supersonic Axial-Flow Compressor in Air. I - Performance of Compressor Rotor at Design Tip Speed of 1600 Feet per Second. NACA RM E7L10, 1948.

8. Boxer, Emanuel, and Erwin, John R.: Investigation of a Shrouded and an Unshrouded Axial-Flow Supersonic Compressor. NACA RM L50G05, 1950.

9. Kantrowitz, Arthur, and Donaldson, Coleman duP.: Preliminary Investigation of Supersonic Diffusers. NACA WR-713, 1945. (Supersedes NACA ACR L5D20.)

10. Johnsen, Irving A., Wright, Linwood C., and Hartmann, Melvin J.: Performance of 24-Inch Supersonic Axial-Flow Compressor in Air. II - Performance of Compressor Rotor at Equivalent Tip Speeds from 800 to 1765 Feet per Second. NACA RM E8G01, 1949.

11. Oswatitsch, Kl.: Pressure Recovery for Missiles with Reaction Propulsion at High Supersonic Speeds (The Efficiency of Shock Diffusers). NACA TM 1140, 1947.

12. Zimney, Charles M., and Lappi, Viola M.: Data for Design of Entrance Vanes from Two-Dimensional Tests of Airfoils in Cascade. NACA WR L-188, 1945. (Supersedes NACA ACR L5G18.)

13. Lieblein, Seymour, and Ackley, Richard H.: Secondary Flows in Annular Cascades and Effects on Flow in Inlet Guide Vanes. NACA RM E51G27, 1951.

14. Gerrish, Harold C., and Meem, J. Lawrence, Jr.: The Measurement of Fuel-Air Ratio by Analysis of the Oxidized Exhaust Gas. NACA Rep. 757, 1943. (Supersedes NACA WR E-128.)

15. NACA Subcommittee on Compressors: Standard Procedures for Rating and Testing Multistage Axial-Flow Compressors. NACA TN 1138, 1946.

16. Ullman, Guy N., Hartmann, Melvin J., and Tysl, Edward R.: Experimental Investigation of a 16-Inch Impulse-Type Supersonic-Compressor Rotor. NACA RM E51G19, 1951.

2897

17. Anon.: Power Test Codes A.S.M.E. 1940. Information on Instruments and Apparatus. Pt. 5, Ch. 4, pub. by Am. Soc. Mech. Eng., 1940.

18. Perry, John H., ed.: Chemical Engineers' Handbook. Second ed., McGraw-Hill Book Co., Inc., 1941.

19. Lown, Harold, and Hartmann, Melvin J.: Investigation of a 24-Inch Shock-in-Rotor Type Supersonic Compressor Designed for Simple Radial Equilibrium Behind Normal Shock. NACA RM E51H08, 1951.

20. Lighthill, M. J.: On boundary layers and upstream influence. I. A comparison between subsonic and supersonic flows. Proc. Roy. Soc. (London), ser. A, vol. 217, no. 1130, May 7, 1953, pp. 344-357.

21. Lieblein, Seymour, Schwenk, Francis C., and Broderick, Robert L.: Diffusion Factor for Estimating Losses and Limiting Blade Loadings in Axial-Flow-Compressor Blade Elements. NACA RM E53D01, 1953.

22. Graham, Robert C., Klapproth, John F., and Barina, Frank J.: Investigation of Off-Design Performance of Shock-in-Rotor Type Supersonic Blading. NACA RM E51C22, 1951.

23. Moeckel, W. E.: Approximate Method for Predicting Form and Location of Detached Shock Waves Ahead of Plane or Axially Symmetric Bodies. NACA TN 1921, 1949.

TABLE I. - COORDINATES OF PITCH SECTION OF ROTOR BLADE

[r = 6.800 in.]

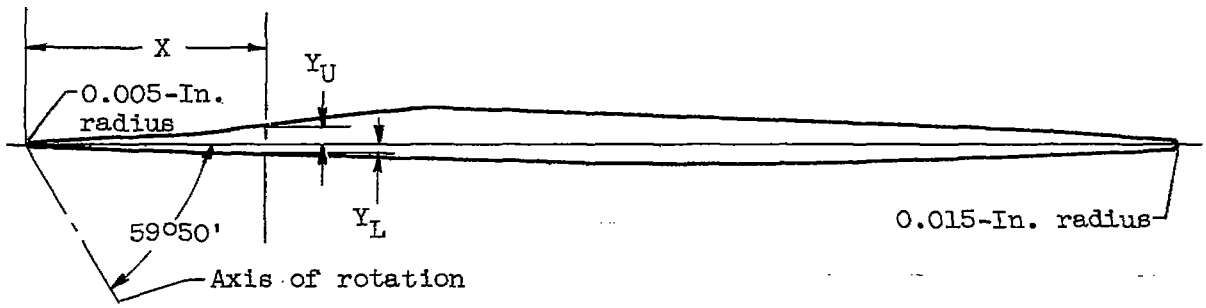

X	Y_L	Y_U	X	Y_L	Y_U
0	0	0.005	2.100	0.065	0.108
.100	.005	.017	2.200	.067	.104
.200	.009	.029	2.300	.067	.100
.300	.013	.033	2.400	.067	.096
.400	.017	.029	2.500	.066	.094
.418	.018	.028	2.600	.065	.090
.500	.020	.035	2.700	.064	.087
.600	.023	.042	2.800	.062	.084
.700	.027	.052	2.900	.060	.080
.800	.030	.064	3.000	.058	.076
.900	.033	.077	3.100	.056	.073
1.000	.036	.090	3.200	.052	.069
1.100	.039	.102	3.300	.049	.064
1.200	.042	.115	3.400	.045	.060
1.300	.045	.127	3.500	.041	.056
1.400	.048	.132	3.600	.037	.050
1.500	.051	.128	3.700	.032	.044
1.600	.054	.125	3.800	.027	.037
1.700	.056	.122	3.900	.021	.029
1.800	.058	.118	4.000	.016	.019
1.900	.061	.114	4.056	0	0
2.000	.063	.111			

NACA

2897

[redacted]

2897

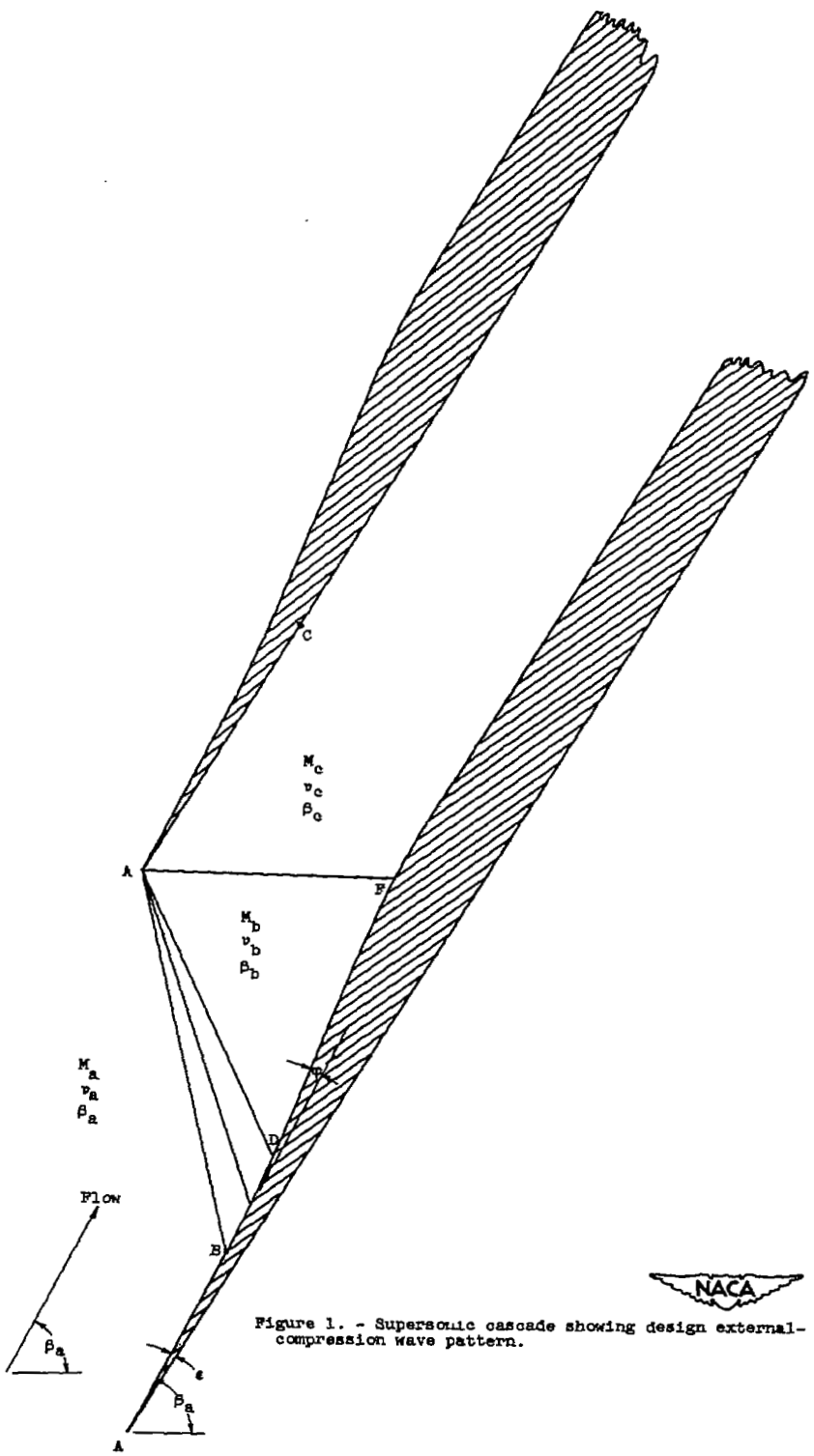

Figure 1. - Supersonic cascade showing design external-compression wave pattern.

2897

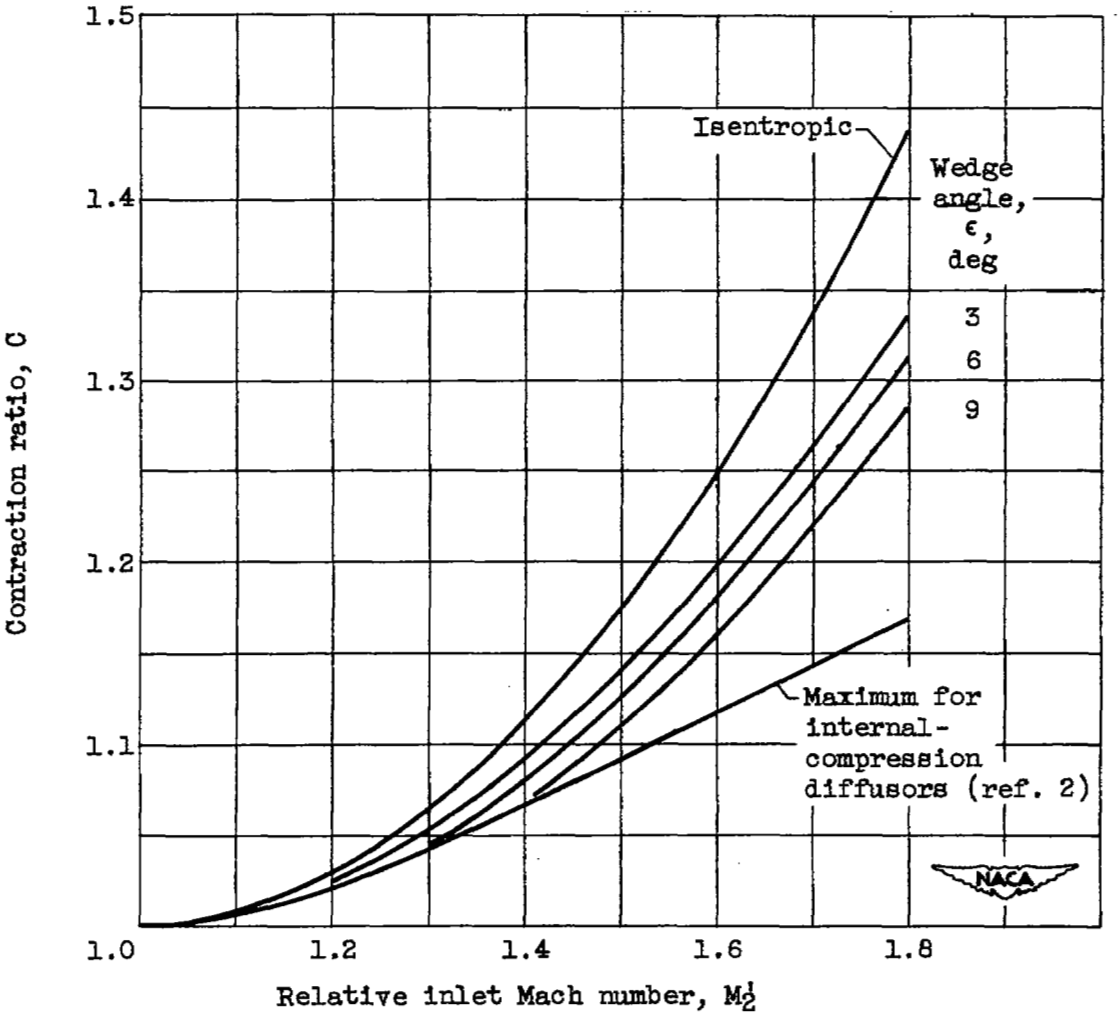

Figure 2. - Effect of varying leading-edge wedge angle on contraction ratio.

2897

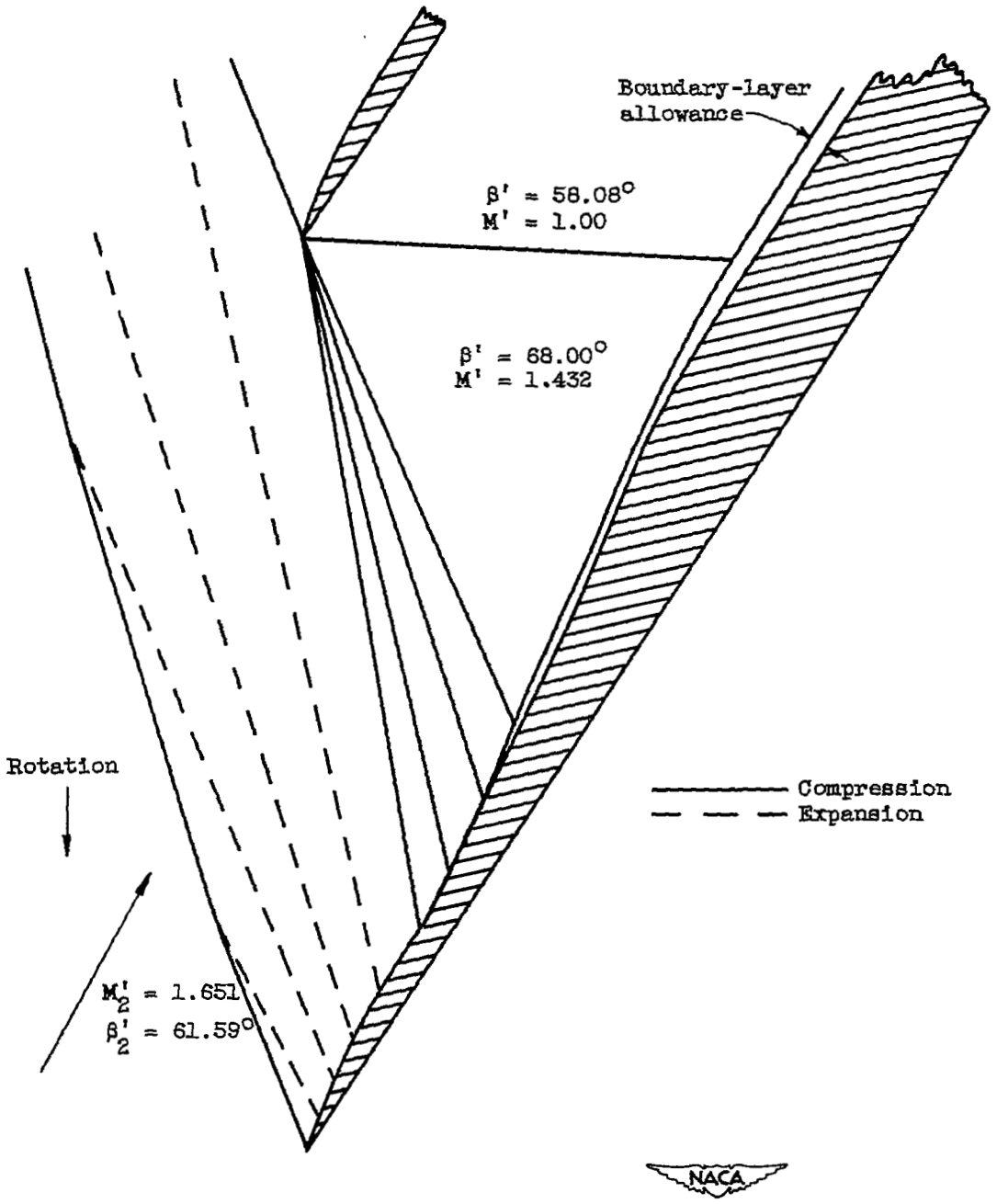

Figure 3. - Pitch section of blade.

[redacted]

2887

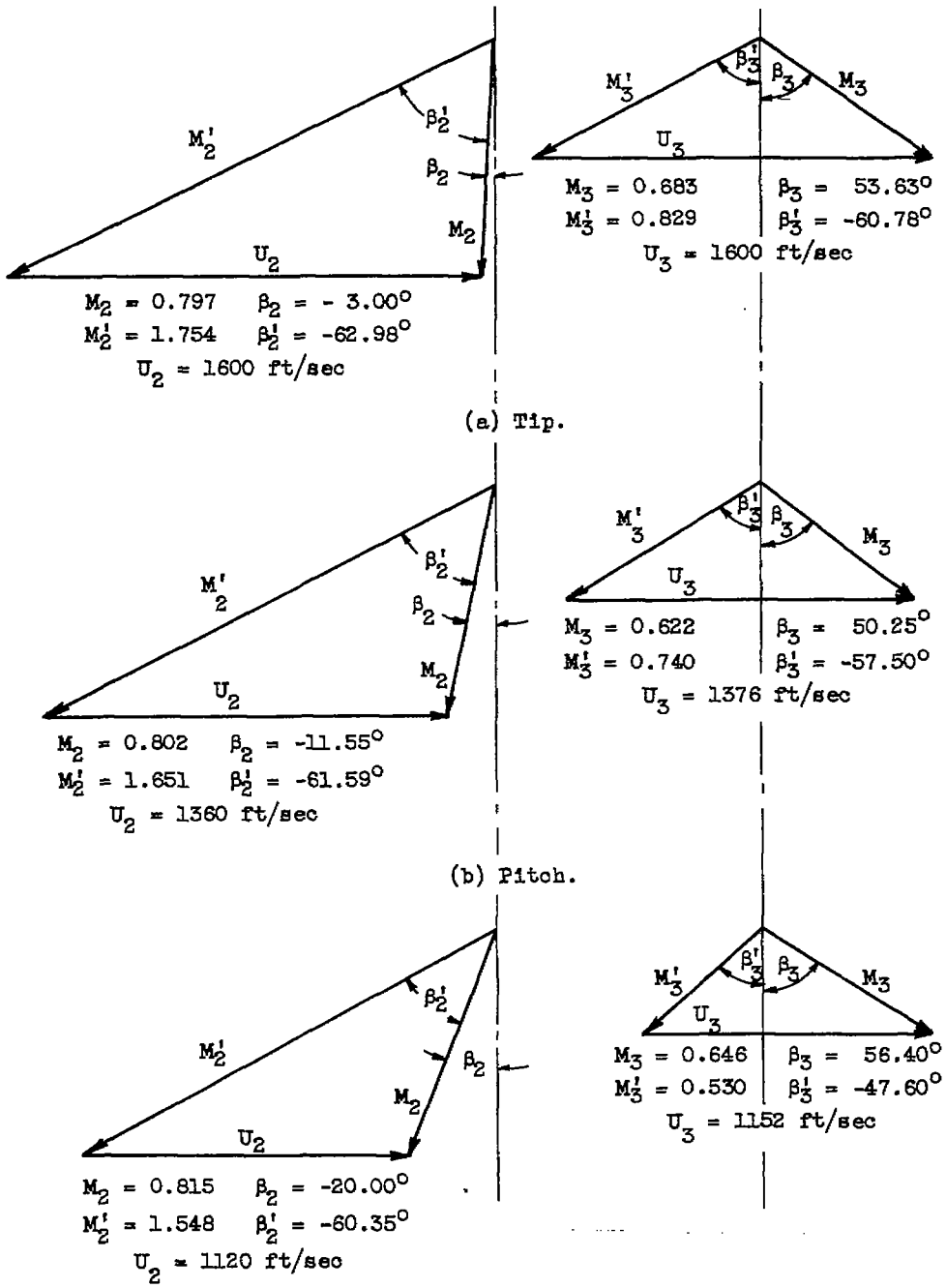

Figure 4. - Design vector diagrams for air at tip, pitch, and root sections of rotor blade.

2897

CW-4

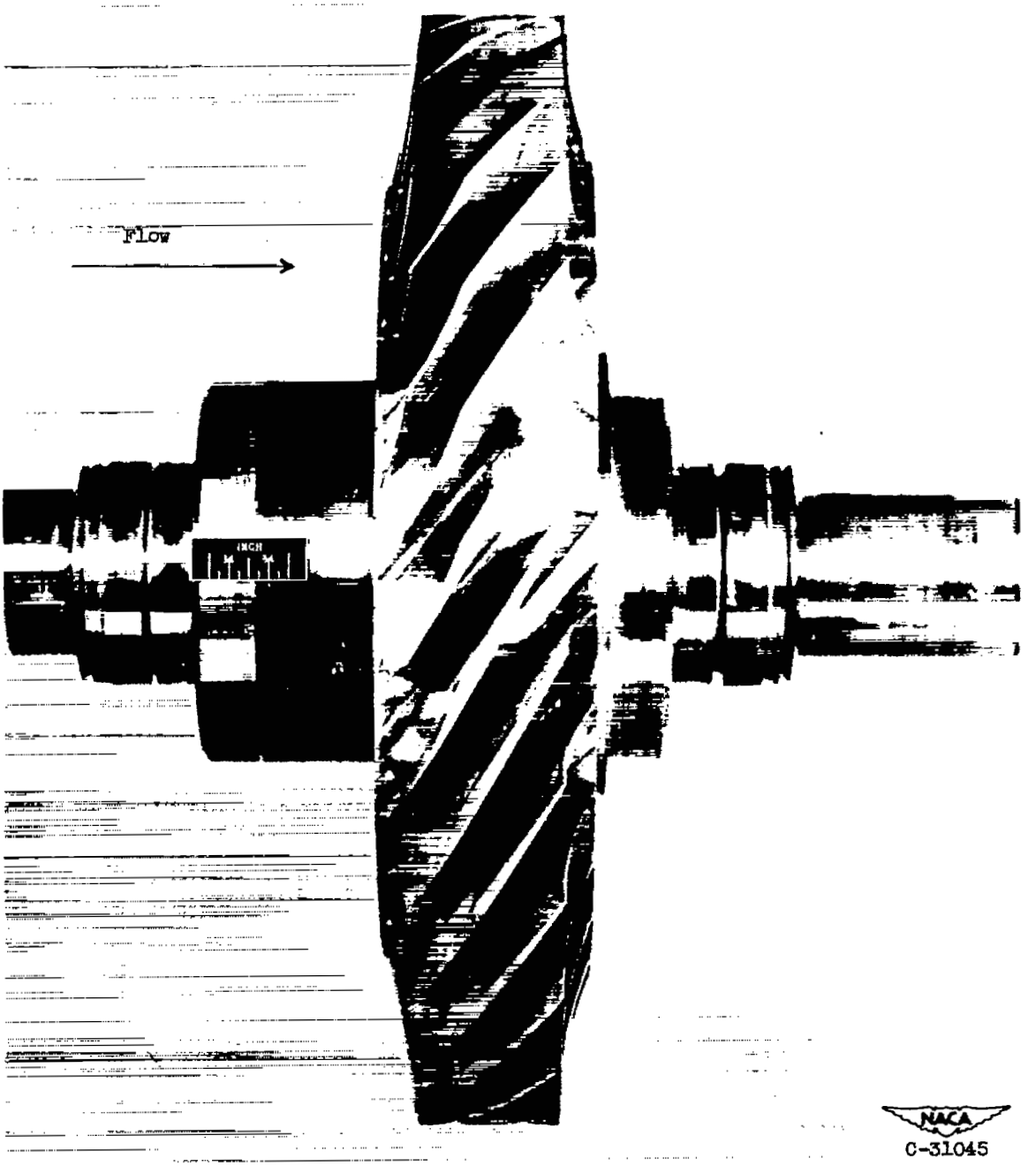

Figure 5. - 16-Inch shock-in-rotor supersonic compressor.

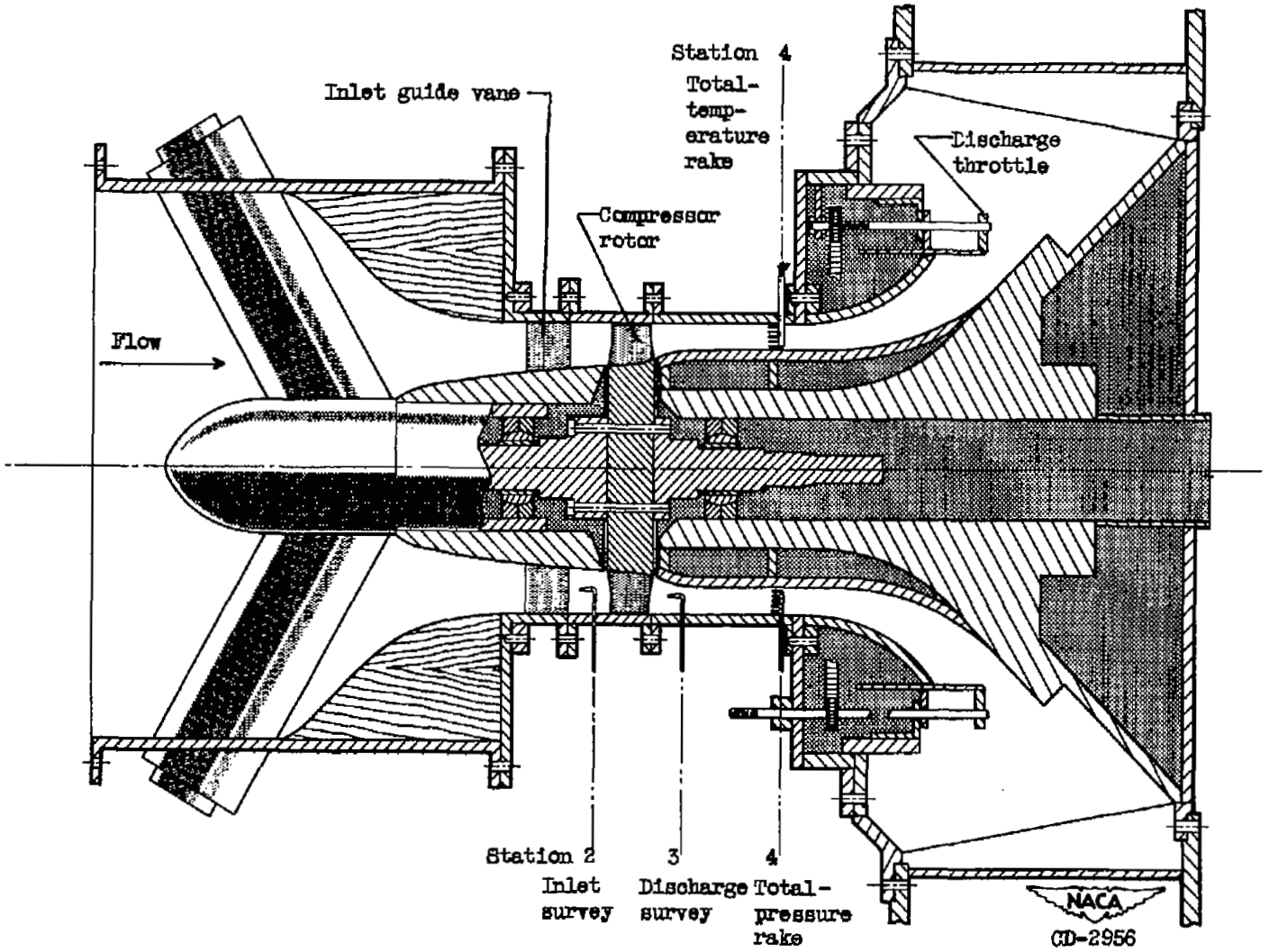

Figure 6. - Schematic diagram of variable-componet compressor test rig.

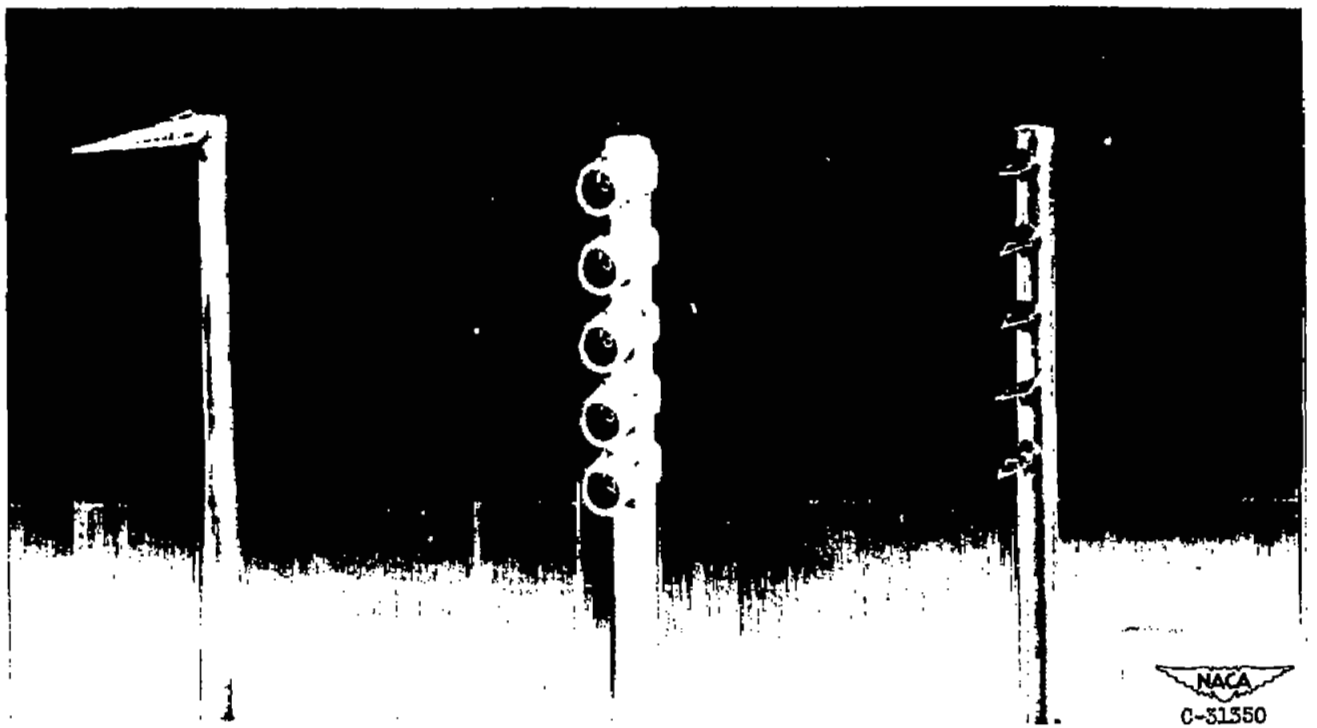

(a) Cone survey probe. (b) Shielded total-pressure rake. (c) Spike-type thermocouple rake.

Figure 7. - Pressure and temperature measuring instruments.

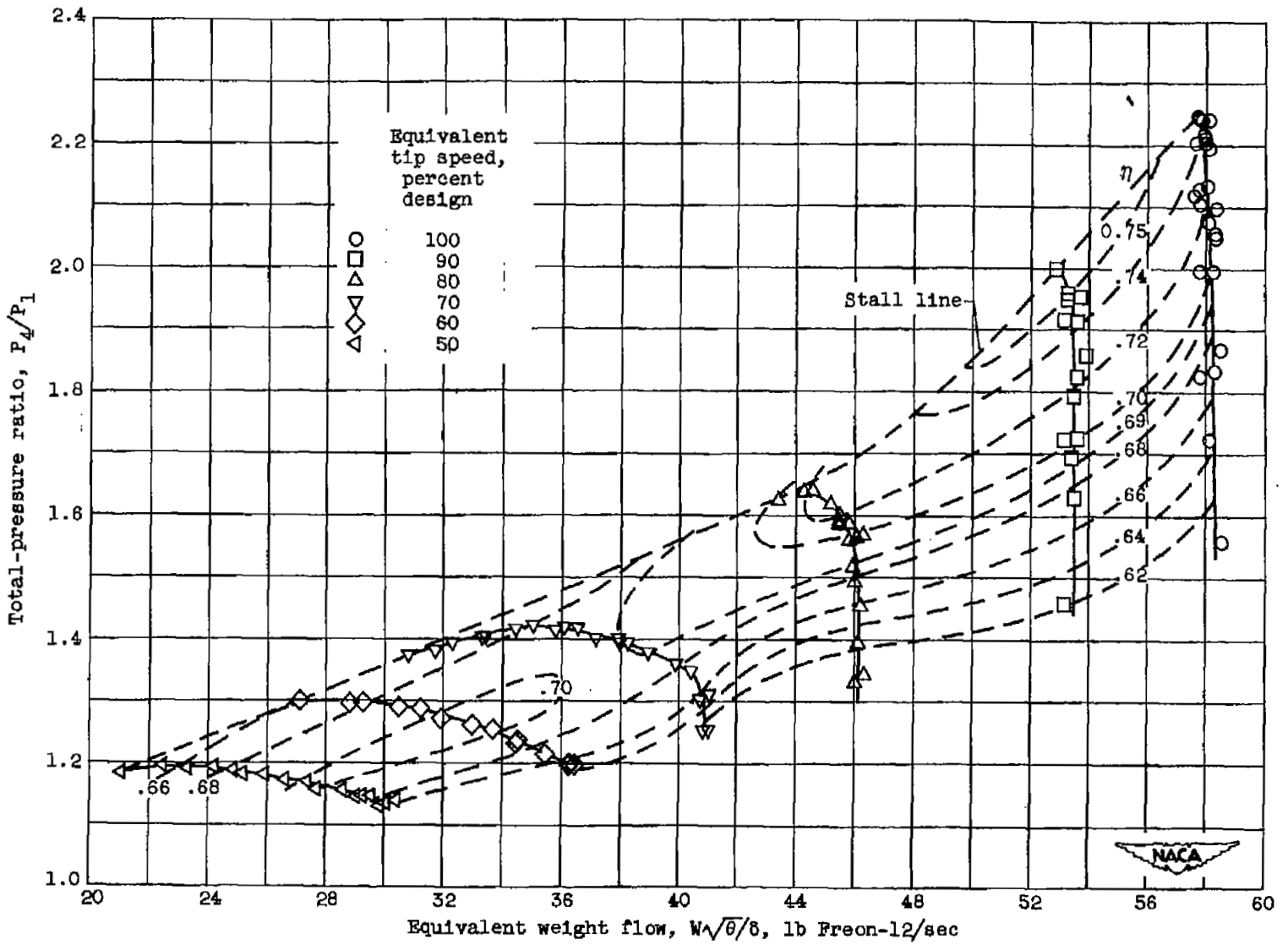

Figure 8. - Over-all performance of 16-inch shock-in-rotor compressor.

2897

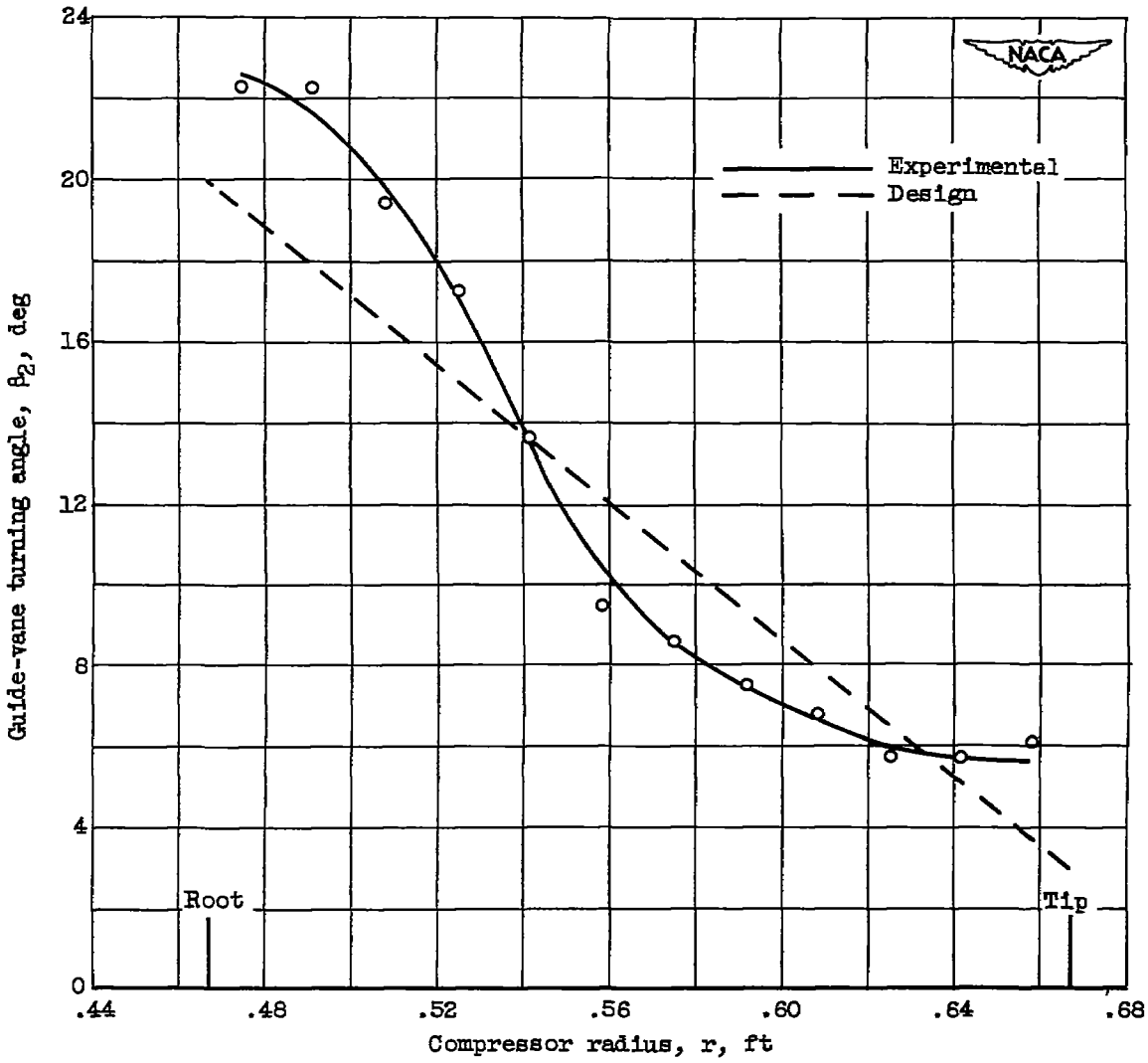

Figure 9. - Variation of guide-vane turning angle with radius at design speed and peak efficiency.

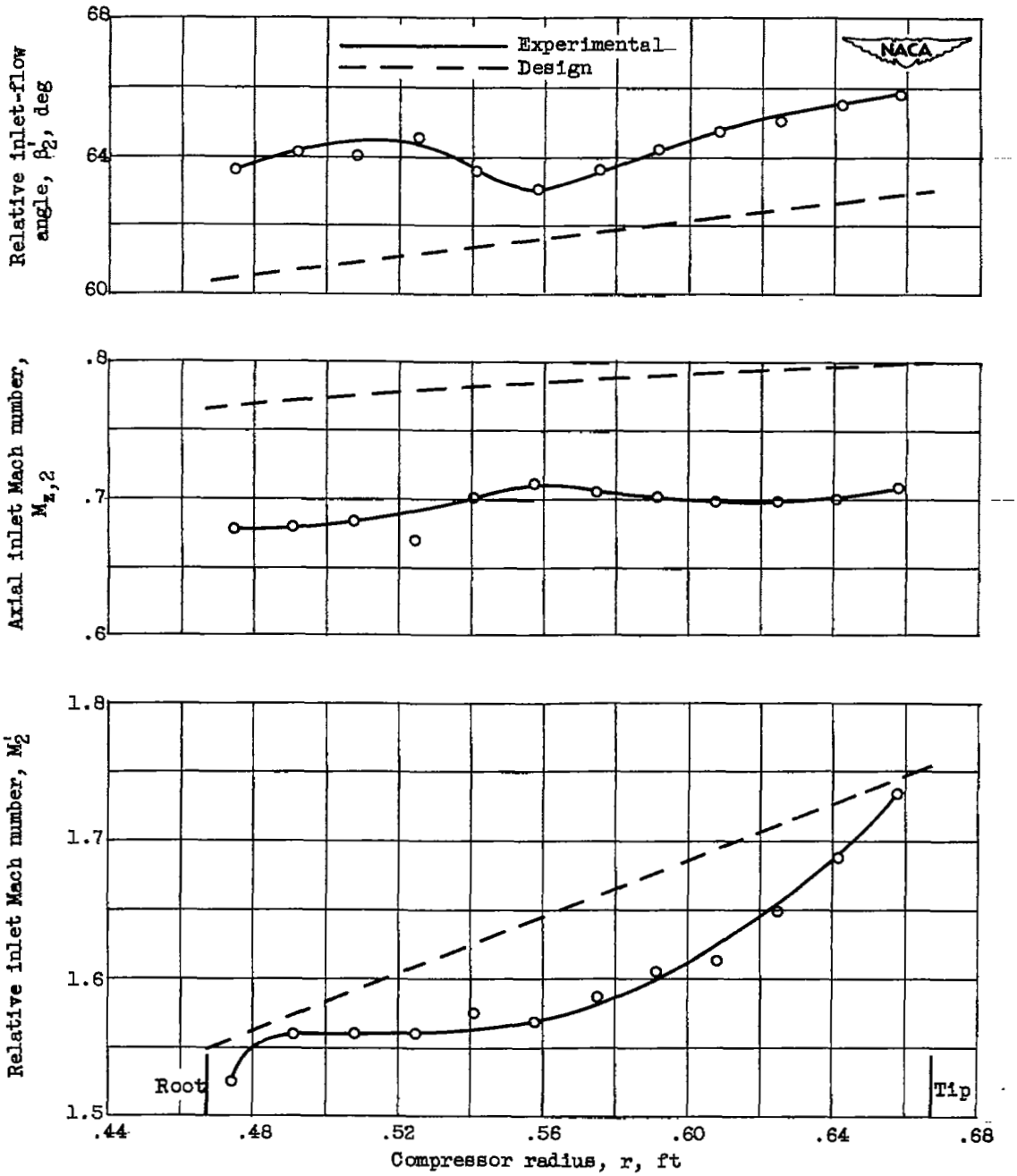

Figure 10. - Rotor-inlet survey at design speed and peak efficiency.

2897

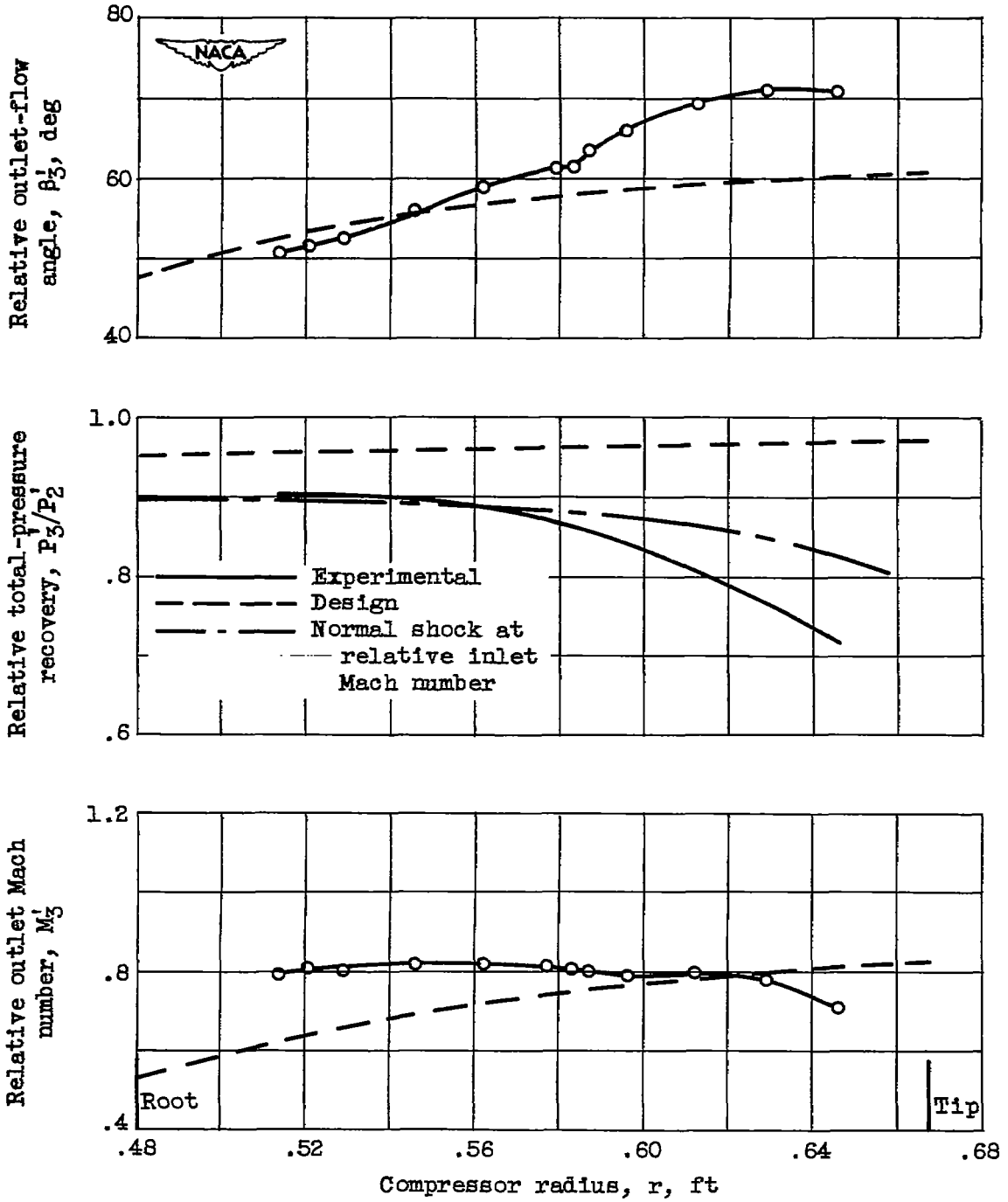

Figure 11. - Rotor-outlet survey at design speed and peak efficiency.

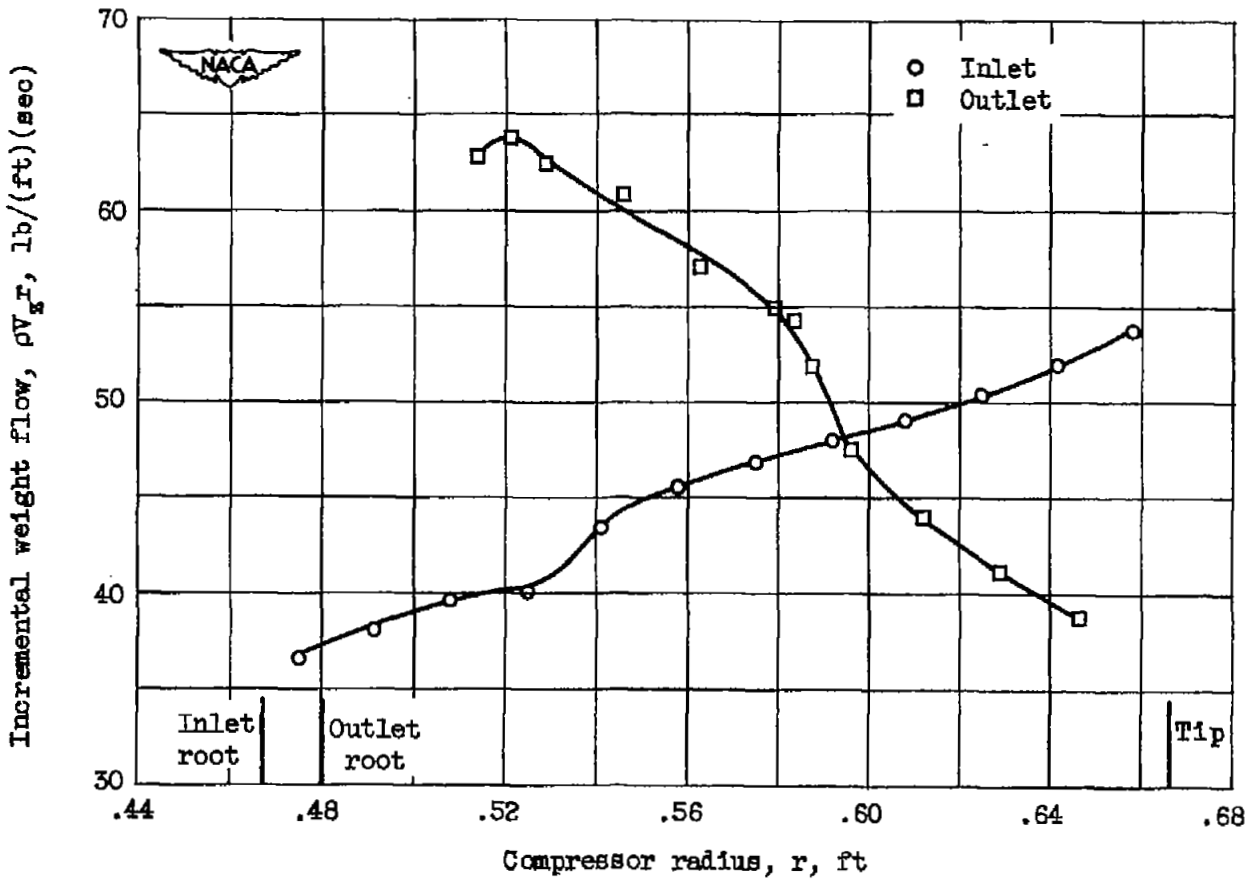

Figure 12. - Weight-flow profiles at compressor inlet and outlet at design speed and peak efficiency.

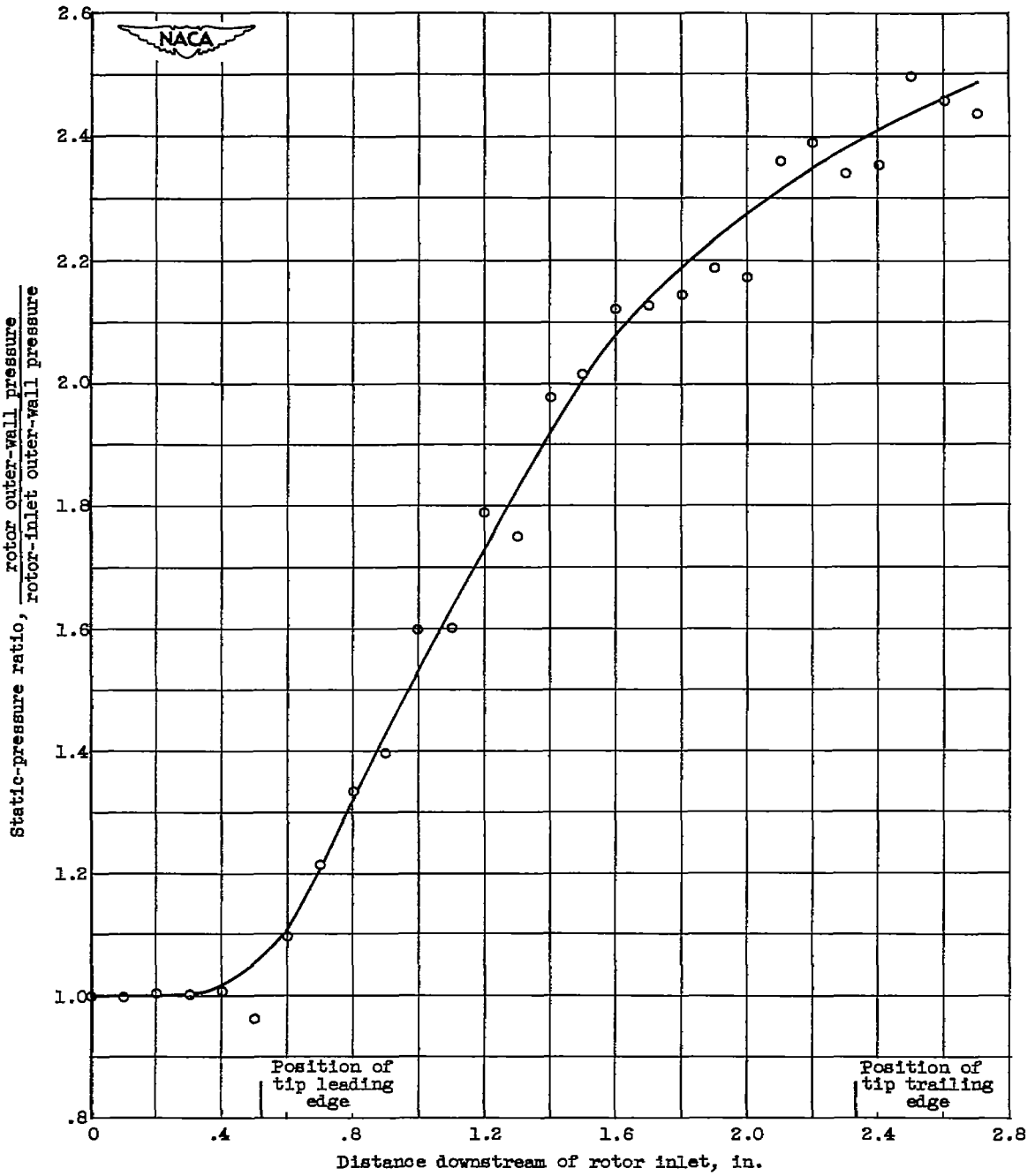

Figure 13. - Static-pressure distribution along compressor outer wall at design speed and peak efficiency.

[redacted]

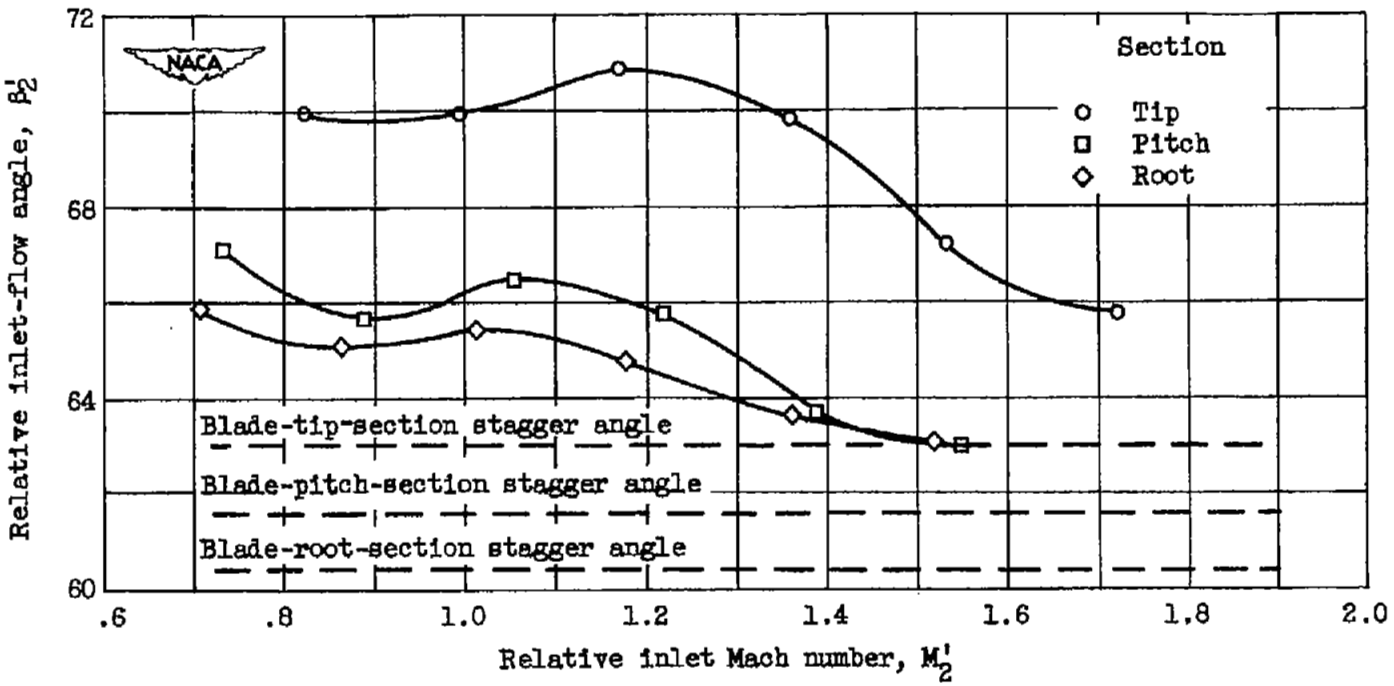

Figure 14. - Effect of relative inlet Mach number on relative inlet-flow angle for maximum weight-flow points at several compressor speeds.

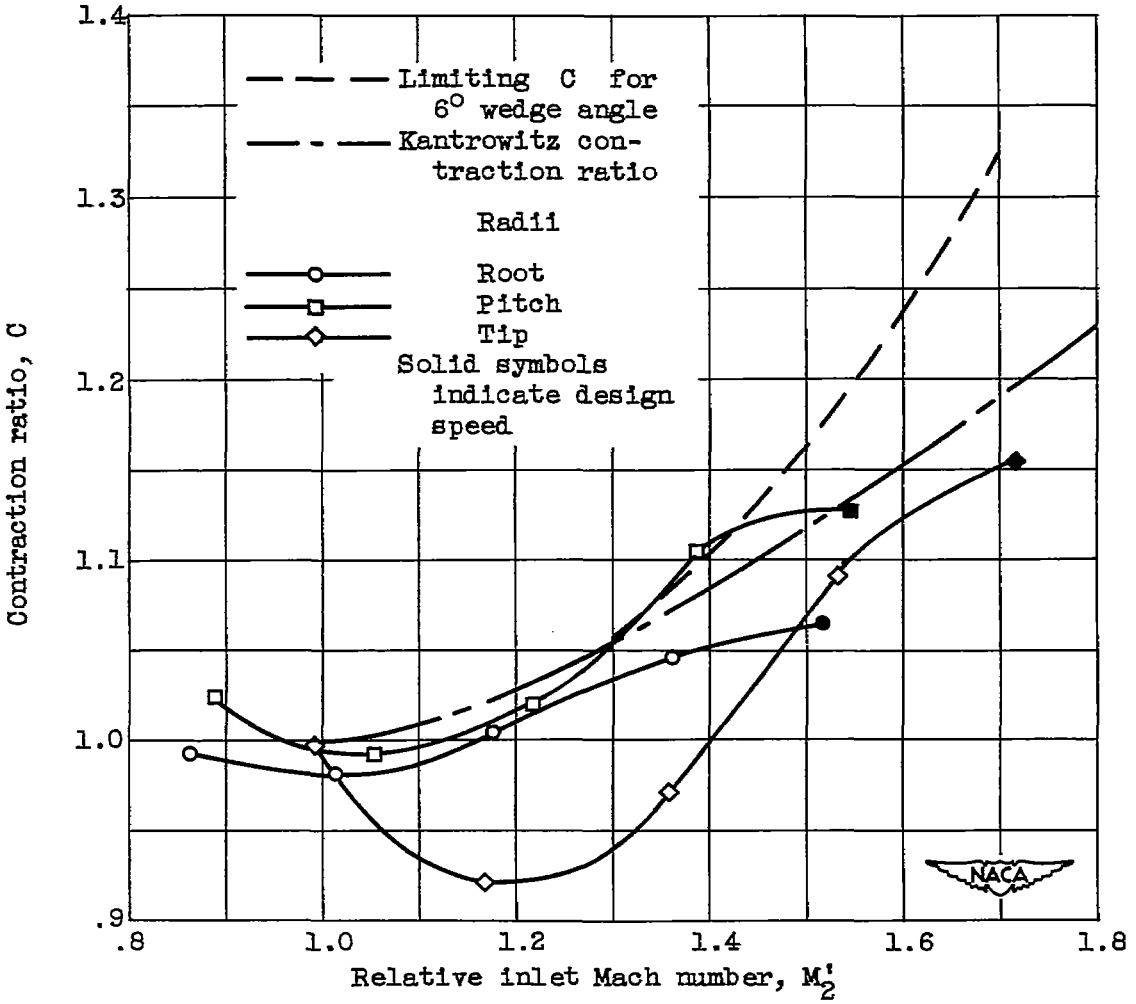

Figure 15. - Comparison of experimental and theoretical values of contraction ratio.

[redacted]

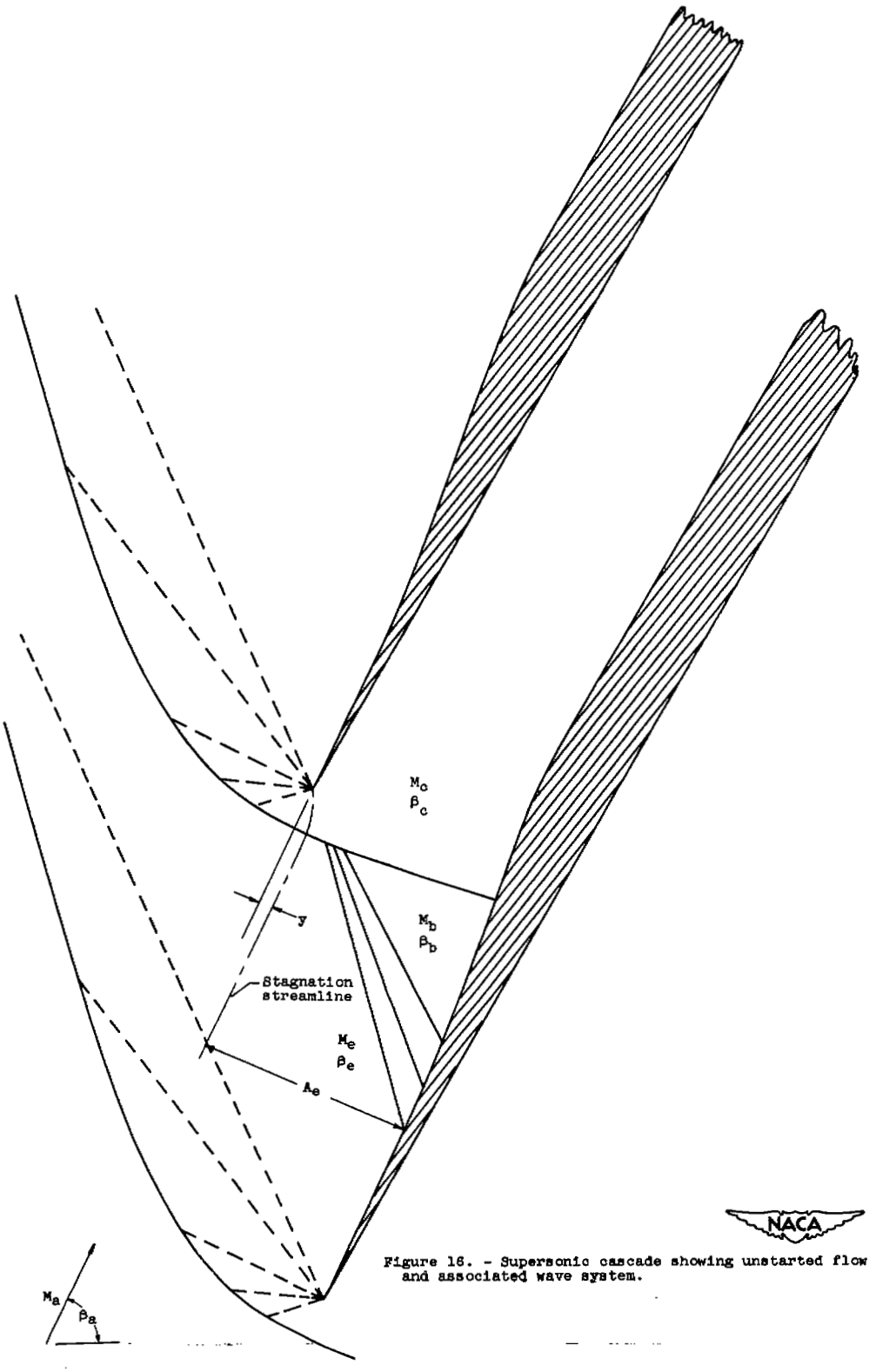

Figure 16. - Supersonic cascade showing unstarted flow and associated wave system.

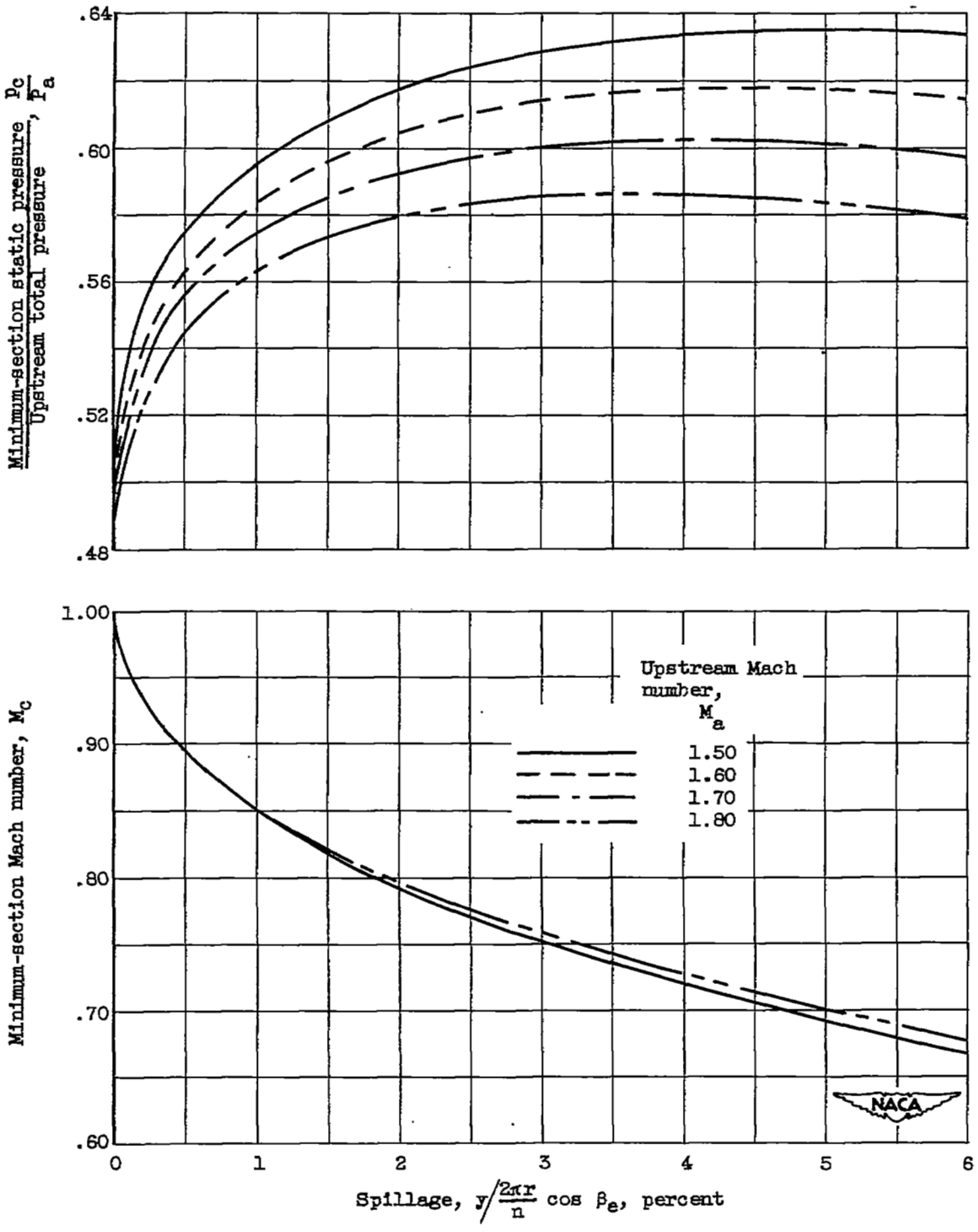

Figure 17. - Effect of spillage on minimum-section Mach number and static pressure for several values of upstream Mach number (M_a, fig. 16).

SECURITY INFORMATION